IEEE Access
Multidisciplinary ⋮ Rapid Review ⋮ Open Access Journal

Received June 12, 2020, accepted June 29, 2020, date of publication July 8, 2020, date of current version August 11, 2020.

Digital Object Identifier 10.1109/ACCESS.2020.3007838

High-Efficiency and Tunable Terahertz Linear-to-Circular Polarization Converters Based on All-Dielectric Metasurfaces

YANZHAO HOU[1], (Member, IEEE), CHAO ZHANG[2,3], AND CHENGRUI WANG[1]

[1]National Engineering Laboratory for Mobile Network Technologies, Beijing University of Posts and Telecommunications, Beijing 100876, China
[2]State Key Laboratory of Information Photonics and Optical Communications, Beijing University of Posts and Telecommunications, Beijing 100876, China
[3]School of Information and Communication Engineering, Beijing University of Posts and Telecommunications, Beijing 100876, China

Corresponding author: Yanzhao Hou (houyanzhao@bupt.edu.cn)

This work was supported in part by the National Natural Science Foundation of China under Grant 61701042, in part by the National Key Research and Development Program of China under Grant 2018YFB2100202, in part by the Research Fundation of Ministry of Education-China Mobile under Grant MCM20180101, and in part by the 111 Project of China under Grant B16006.

ABSTRACT Terahertz polarization converter has drawn great attention for its properties of wavefront control in recent years. However, the low transmission efficiency of these converters remains a major obstruction to be resolved. A promising solution is the all-dielectric metasurface, based on which, this study proposes a high-efficiency transmissive terahertz linear-to-circular polarization converter. The simulations show the transmission efficiency of the converter is beyond 88% with an ellipticity < -0.8 from 0.555 to 0.737 THz, and the maximum efficiency even reaches 100% at 0.660 THz. Furthermore, the converter can also be actively manipulated by combining with dynamic material. The frequency sensitivity is 98 GHz/100K, and the modulation depth of ellipticity at 0.725 THz exceeds 76%. The excellent performances of these converters offer more potentials for terahertz devices.

INDEX TERMS Metamaterials, optical materials.

I. INTRODUCTION

The polarization manipulation of terahertz (THz) wave is one of the most significant functions in the development of THz devices [1]–[9]. Among various THz waves with different polarization states, the THz circularly polarized wave, for its robustness and chirality [10], has been manifested in a wide range of optical applications, such as 6G wireless communication, drug detection and biomolecules sensing [11]–[13]. However, the states of most electromagnetic waves generated from THz emitters are linearly polarized [14], and the function of corresponding polarization converters are just linear to cross [15]–[16]. Therefore, it is becoming increasingly difficult to ignore the realization of THz linear-to-circular polarization conversion. Albeit the excellent performance of wave plates and lenses have exhibited in polarization conversion, their bulk size and limited choice of materials still hamper the progress of THz integrated devices. Conversely, as the two-dimensional artificial engineering material with unique electromagnetic properties, metasurfaces have excellent abilities to control the phase, amplitude, and polarization conversion of THz wave without the mentioned problems [17]–[21].

By carefully designing geometric parameters, various transmissive or reflective metallic metasurfaces have been proposed to realize THz linear-to-circular polarization conversion. For example, Jiang *et al.* proposed a high-efficiency reflective linear-to-circular polarization converter based on a metallic split ring metasurface, and the reflection efficiency can exceed 88% in the frequency range of 0.60-1.41 THz [22]. Fahad *et al.* carried out several investigations into a broadband transmissive linear-to-circular polarization converter with diagonally symmetric structure, and the transmission efficiency varied from 50% to 80% within a wideband range of about 0.53 THz [23]. However, although high efficiency reflective linear-to-circular polarization converters are relatively easy to design and manufacture in the THz region [24], [25], perhaps some serious disadvantages still hamper their development. One of the limitations with these structures is that incident electromagnetic waves may interfere with the reflection waves and influence quality of the output signal. Another problem is the inconvenience

The associate editor coordinating the review of this manuscript and approving it for publication was Pu-Kun Liu.

in practical applications. As for the transmissive polarization converters, although without these problems, the inherent ohmic losses of metals and the large reflection losses make it difficult to achieve high efficiency at THz frequency. For the purpose of designing high-efficiency and convenient THz devices, all-dielectric metasurface is employed for its Mie-resonance to simultaneously resolve all the problems [26].

Although metasurfaces have provided new options for controlling polarization, the operating frequency and polarization output of these converters are still confirmed by their geometrical parameters. The potential of various applications that require dynamical control over the polarization of electromagnetic waves has been limited. Therefore, the realization of a tunable polarization converter has been thought of as a key factor in expanding the practical applications of THz devices. In order to achieve this goal, we employ the hybrid metasurfaces whose unit cell is combined with active material. The electromagnetic properties and resonance responses of these metasurfaces can be dynamically controlled under external stimuli. As previous studies reported, a great variety of active materials have been incorporated with metasurfaces, such as liquid crystals, graphene, phase change materials, and semiconductors [27]–[30]. Among them, the semiconductor indium antimonide (InSb), whose carrier concentration will change greatly under thermal stimulation, is receiving renewed interest in all-dielectric hybrid metasurfaces. Therefore, the tunable all-dielectric hybrid metasurface based on InSb can become a promising choice for active and high-efficiency THz devices.

Here, we propose a high-efficiency transmissive linear-to-circular polarization converter based on the all-dielectric silicon metasurface. The anisotropy of silicon pillars on the silica substrate provides enough freedom to manipulate polarization conversion. Through simulation, the operating frequency of the converter ranges from 0.555 to 0.737 THz with an absolute value of axis ratio (AR) < 3 dB, and transmission efficiency > 88% are realized. It is worth emphasizing that a perfect left-handed circularly polarized wave is achieved at 0.66 THz, and the corresponding transmission efficiency can reach 100%. Besides, the converter can also be actively manipulated by combining with active InSb film. Numerical simulation demonstrates that the frequency sensitivity of the tunable converter is 98 GHz/100K, and the ellipticity of the circularly polarized THz wave can be tuned from −1.00 to −0.24 at 0.725 THz. All of these excellent performances indicate the potential applications of the converter in high-efficiency THz devices.

II. DESIGN, THEORY AND RESULTS DISCUSSION

Absorption loss is well known as one of the main factors that affect the efficiency of the transmissive metasurface. In order to reduce the impact of this point, doped silicon is chosen as structure material due to its high permittivity (11.7) and low loss tangent (0.0001) [31]. As illustrated in Fig. 1(a), the tunable THz linear-to-circular polarization converter is

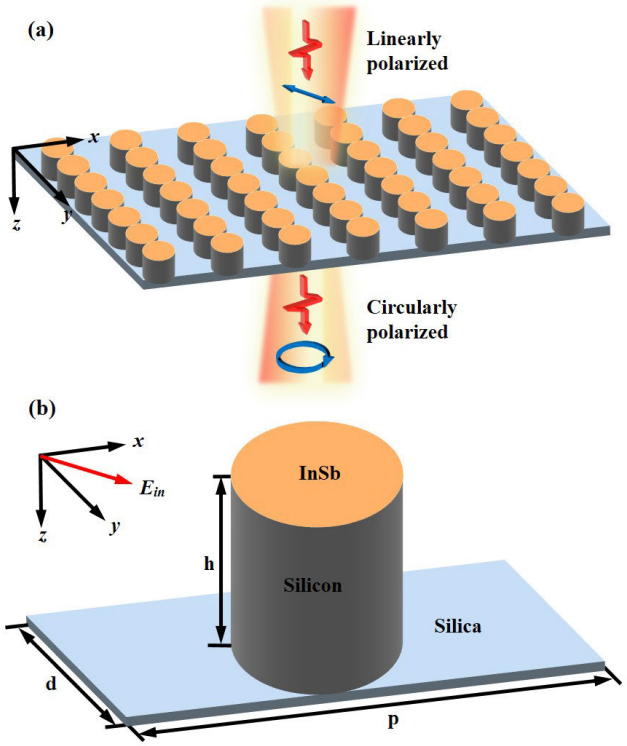

FIGURE 1. Schematic diagram of the tunable polarization converter. (a) Schematic of the converter consists of a silica substrate, periodic silicon pillars, and indium antimonide (InSb) film deposited on the pillars. (b) Illustration and geometric parameters of the unit cell.

based on a serious of tangential silicon pillars on the silica substrate (with a thickness of 10 μm). For the purpose of dynamically controlling the polarization converter, the InSb film is deposited on the silicon pillars, as shown in Fig. 1(b). The corresponding structure parameters are set to period p = 250 μm, diameter d = 60 μm, and height h = 90 μm. In this case, the polarization of the electric field regarding the incident wave is 45° relative to the x-direction. Through simulation and structural optimization, perfect circularly polarized waves can be achieved under the normal incidence of THz linearly polarized waves.

Firstly, the all-dielectric polarization converter without InSb film is simulated using a frequency-domain solver in CST Microwave Studio. The unit cell boundary conditions are employed to characterize the periodic structure of the converter. As demonstrated in Fig. 1(b), the plane wave with a normal incidence and the $45^{c}irc$ polarized electric field is selected as the excitation source. For data management and analysis, the transmissive electromagnetic wave of the converter can be expressed as $E_t = E_{xt}e_x + E_{yt}e_y = t_{xx}exp(j\varphi_{xx})E_{xi}e_x + t_{yy}exp(j\varphi_{yy})E_{yi}e_y$, where $t_{xx} = |E_{xt}/E_{xi}|$ and $t_{yy} = |E_{yt}/E_{yi}|$ represent the transmission coefficient of x-x and y-y polarization conversion, respectively. Corresponding, φ_{xx} and φ_{yy} are the transmission phase for the two orthogonal components. It has been demonstrated that when $t_{xx} = t_{yy}$ and $\Delta\varphi = \varphi_{yy} - \varphi_{xx} = 2n\pi \pm 0.5\pi$ are satisfied simultaneously, the perfect linear-to-circular

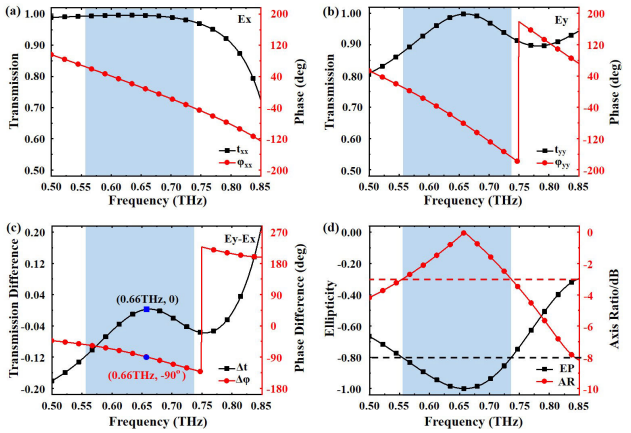

FIGURE 2. Simulated results of the all-dielectric terahertz (THz) linear-to-circular polarization converter. (a) The transmission coefficient and phase of the x-polarized component. (b) The transmission coefficient and phase of the y-polarized component. (c) The difference in transmission coefficient and phase between two orthogonal components. (d) The ellipticity (EP) and axial ratio (AR) of the designed converter.

polarization conversion can be achieved [31]. The simulated transmission coefficients and phases of the orthogonal components are plotted in Fig. 2(a) and Fig. 2(b), respectively. To quantitatively analyze the relationship between these two components, the difference in transmission coefficient and phase between them is plotted in Fig. 2(c). It is obvious that the amplitudes of t_{xx} and t_{yy} are equal, and the phase difference is $-90°$ at 0.66 THz. Combining this result with the above theory, it can be speculated that the perfect circularly polarized wave is realized. To verify this result, stokes parameters are introduced to describe the polarization states of the transmission THz wave [22].

$$I = |t_{xx}|^2 + |t_{yy}|^2 \tag{1}$$
$$Q = |t_{xx}|^2 - |t_{yy}|^2 \tag{2}$$
$$U = 2|t_{xx}||t_{yy}|cos\Delta\varphi \tag{3}$$
$$V = 2|t_{xx}||t_{yy}|sin\Delta\varphi \tag{4}$$

The normalized ellipticity is defined as V/I to characterize the polarization conversion performance of the designed structure, where $V/I = -1$ and $V/I = +1$ indicate that the transmission signals are perfect left-handed or right-handed circularly polarized waves, respectively.

Based on Eq. (1) and Eq. (4), the normalized ellipticity of the converter is plotted with a black curve in Fig. 2(d). The ellipticity less than -0.8 in the frequency range from 0.555 to 0.737 THz (the blue shaded region), suggesting that the proposed converter has an excellent performance in polarization conversion. In addition, the axial ratio (AR) of the transmission wave is also calculated through $AR = 10logtan(\beta)$, where $\beta = 0.5arcsin(V/I)$. As shown by the red curve in Fig. 2(d), the absolute value of AR is less than 3 dB in the range of 0.555 to 0.737 THz, which also illustrates the high conversion performance of the converter. The most obvious finding to emerge from this graph is that the ellipticity equal to -1 at 0.66 THz, this phenomenon is consistent with the speculations from Fig. 2(c). Furthermore, the proposed structure performs well in the linear-to-circular polarization conversion with a bandwidth of about 0.182 THz, which expands its application range and robustness in THz communication devices.

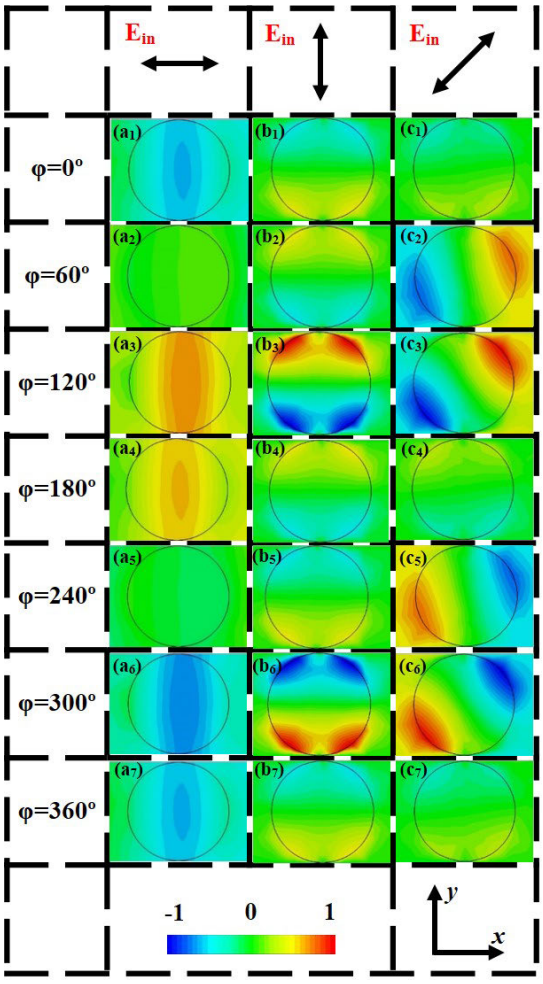

FIGURE 3. Simulated electric field distribution of the proposed converter for different time phases. (a) Excited by the x-polarized plane wave. (b) Excited by the y-polarized plane wave. (c) Excited by the 45^c *irc* polarized plane wave.

In order to understand the underlying physical mechanism of the THz polarization converter, our main results of the electric field evolution process under the time phase are shown in Fig. 3. The frequency of the perfect circularly polarized wave is selected as the frequency for observing the electric field distribution. When the converter is excited by the x-polarized plane wave, the simulated results are indicated in Figs. 3(a_1)$-$3(a_7). It is apparent that a weak electric resonance mode can be observed. This phenomenon may explain the little influence of the converter on the transmission coefficient of the x-polarized incident wave, that is, the amplitude of t_{xx} is 1 in broadband of about 0.2 THz in Fig. 2(a). In contrast, a different resonance mode can

be observed under the incidence of the y-polarized plane wave. One significant evidence from Figs. 3(b_1)−3(b_7) is the accumulated electric field at the edge of the silicon pillar along the y-direction. This phenomenon provides compelling evidence for the magnetic dipole resonance excited in the silicon pillars. The low radiative loss caused by the magnetic resonance results in the high transmission efficiency of the incident wave, as shown in Fig. 2(b) above. The difference between the electric field distribution in the two orthogonal polarized waves is resulted from the anisotropy of the structure, which is also the fundamental reason for the realization of polarization conversion. Further research will explore the electric field distribution of the transmissive left-handed circularly polarized wave under the 45$^c irc$ polarized plane wave. A perfect left-handed circularly electric field rotation can be observed through the change of time phase, as indicated in Figs. 3(c_1)−3(c_7). This result is consistent with Fig. 2(d) and verifies the correctness of the theoretical calculation. In addition, the magnetic resonance inside the silicon pillars may lead to high transmission efficiency of the converter.

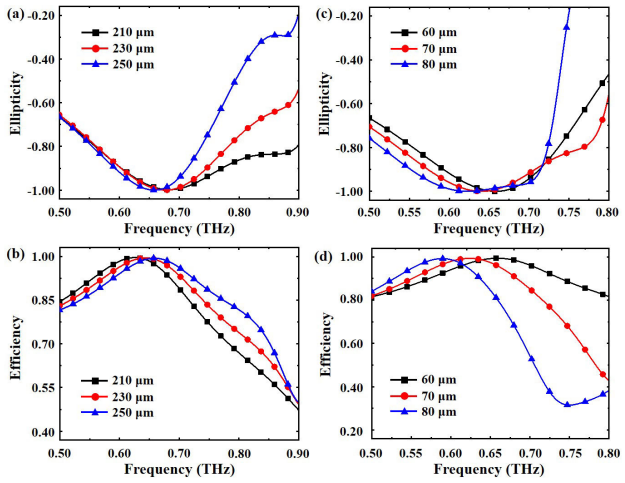

FIGURE 4. The polarization conversion performance of the converters with different geometric parameters. The period-dependent transmission (a) ellipticity and (b) energy efficiency. The diameter-dependent transmission (c) ellipticity and (d) energy efficiency.

For the purpose of giving deep insight into the THz polarization converter performance, $\rho = (|t_{xx}|^2 + |t_{yy}|^2)/2$ is introduced to quantitatively calculate and analyze its transmission energy conversion efficiency. As we expected, the transmission efficiency can reach 100% at 0.66 THz, as seen from the blue curve in Fig. 4(b). It seems possible that this result is due to the magnetic resonance inside the silicon pillars. Furthermore, the transmission efficiency still greater than 88% in the frequency range with ellipticity less than −0.8. Both of these results exhibit the high transmission efficiency of the polarization converter that is difficult to achieve in previous reports.

It is well known that the electromagnetic properties of metasurfaces mainly depend on their design and geometry parameters. As the electric field distribution indicated in Fig. 3, the linear-to-circular polarization conversion is generated from the anisotropy of the designed structure. As shown in Fig. 1(a), the silicon pillars are tangent in the x-axis direction, in contrast, there is a certain pitch in the y-axis direction. The difference of effective permittivity in the two orthogonal directions is the source of all phenomena. Therefore, we further simulate and investigate the variation in the ellipticity and transmission efficiency of the converter under different periods and diameters. Fig. 4(a) shows the ellipticity of the polarization converter under the modulation of period (fixed diameter = 60 μm). When the period increases from 210 μm to 250 μm, the frequency of the ellipticity peak decreases from 0.675 to 0.660 THz. Corresponding, the bandwidth of the ellipticity (ellipticity < −0.8) decreases from 0.337 THz to 0.182 THz. A possible explanation for this might be that as the increases of period, the relative permittivity in the y-axis direction will decrease, which increases the anisotropy between x and y direction. In addition, the transmission energy conversion efficiency is also studied under different periods, as indicated in Fig. 4(b). In contrast to the redshift of ellipticity, the peak of transmission efficiency exhibits a blue shift with the increase of period. Another more significant findings to emerge from this study is that the transmission efficiency peak remains almost constant in various periods. In this case, it can be concluded that all the converters with different periods can achieve high transmission efficiency. However, it is worth noting when the period is confirmed, only one structure can achieve a transmission efficiency of 100% and the ellipticity equals -1. This structure (period = 250 μm, diameter = 60 μm) is what we used in Fig. 2 to investigate the working mechanism of the polarization converter. Apart from the period, the effects of silicon pillar diameter (fixed period = 250 μm) on the converter performance are also investigated in Figs. 4(c)-4(d). There is a redshift of the ellipticity peak is observed with the increase of diameter, and a similar phenomenon also emerges in the transmission efficiency. Combining with the finding in Figs. 4(a)-4(b), this result provides more freedom for the design of the THz polarization converter.

After investigating the perfect conversion performance and high transmission efficiency of the converter, the tunable THz polarization converter is also proposed to expand its application range. The active InSb film is selected to be integrated with the silicon pillars with the aim of tuning the polarization converter electromagnetic response, as illustrated in Fig. 1(b). As an active semiconductor, the permittivity of InSb film can be easily tuned with the increase of temperature, which can be attributed to its small bandgap, high electron-mobility, and the low effective mass. Drude model is also introduced to understand the permittivity of InSb film with various temperatures [32].

$$\varepsilon(\omega) = \varepsilon_\infty - \omega_p^2/(\omega^2 + i\gamma\omega) \tag{5}$$

where ω is the resonant frequency of the InSb, $\varepsilon_\infty = 15.68$ represents its high-frequency value, and the damping constant $\gamma = 0.1\pi$ THz. In addition, the plasma frequency ω_p can be

calculated by the equation:

$$\omega_p = \sqrt{(Ne^2/\varepsilon_0 m)} \tag{6}$$

in which m represents the effective mass of free carriers, and ε_0 is the vacuum permittivity. As a function of temperature, the intrinsic carrier density N of InSb film can be adequately described $N = 5.76 \times 10^{14} T^{3/2} exp(-0.13/kT)$. Through these equations, we can conclude that the permittivity of InSb is indeed closely related to the environmental temperature. As shown in Fig. 5(a), in the frequency of 0.60-0.85 THz, when the temperature rises from 340 K to 400 K, the real part of the permittivity changes more than 470, and the maximum value even reaches 940 at 0.60 THz. Fig. 5(c) shows a similar phenomenon in the imaginary part of the InSb permittivity. All of these findings exhibit the excellent thermal tunability of this active semiconductor, that is why this active material is selected in combination with the polarization converter. Finally, the relative permittivity of the all-dielectric converter can also be tuned due to the influence of the active InSb film.

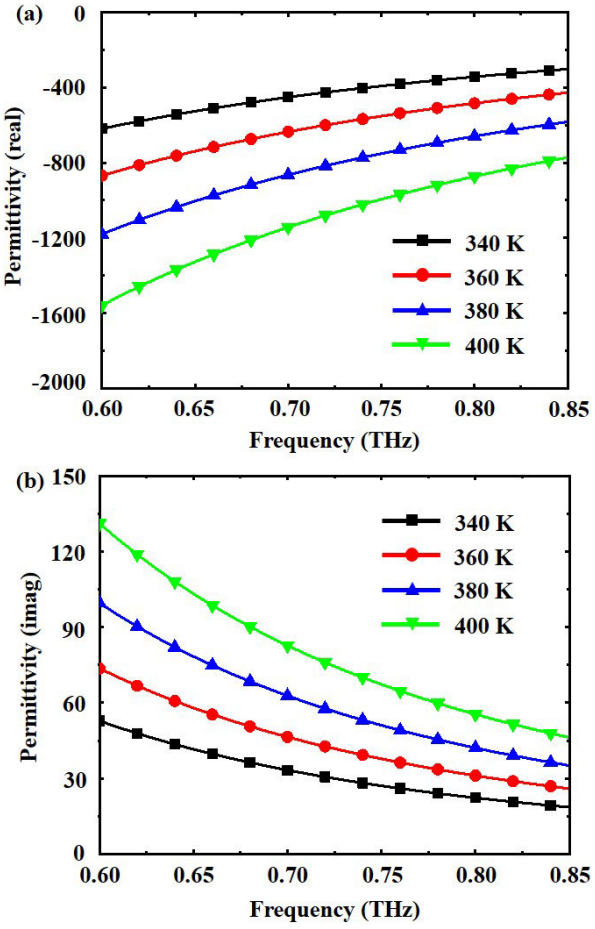

FIGURE 5. The permittivity of the InSb film with different temperatures. The (a) real part and (b) imaginary part of permittivity when the temperature is increased from 340 K to 400 K.

After combining the InSb film (1 μm) with the silicon pillars, the performance of the tunable THz polarization converter with different temperatures is simulated, as shown

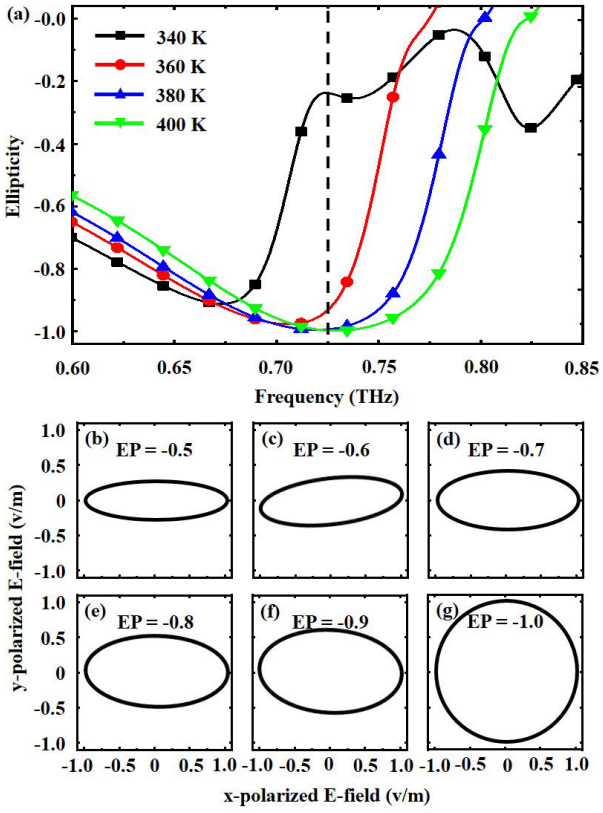

FIGURE 6. The simulated tunability of the THz polarization converter. (a) The ellipticity of the converter under different temperatures. (b-c) The normalized wavefront trajectories for different temperatures at 0.725 THz (corresponding to the dotted line in (a)).

in Fig. 6(a). When the temperature varies from 340 K to 400 K, the peak of ellipticity shifts from 0.672 THz to 0.731 THz. In order to clearly exhibit the tunable performance of the polarization converter, the sensitivity $(f_{max} - f_{min})/(T_{max} - T_{min})/$ is employed and high sensitivity indicates the better tunable performance. It can be calculated that the sensitivity of the converter can reach 98 GHz/100K, which has never been found in the all-dielectric polarization converter. The ellipticity peak still less than -0.8 at different temperatures, this finding demonstrates the excellent polarization conversion performance of the converter in the process of thermal regulation. In the same condition, the amplitude of ellipticity at 0.725 THz increases from -1.00 to -0.24, and the modulation depth can reach 76%. To give a deep insight into the ellipticity regulation, the vector wave equation is introduced as [33]:

$$(\frac{x}{A_{TE}})^2 + (\frac{x}{A_{TE}})^2 - 2(\frac{xycos(\Delta\varphi)}{A_{TE}A_{TM}}) = sin^2(\Delta\varphi) \tag{7}$$

where A_{TE} and A_{TM} represent the transmission coefficient under the x-polarized and y-polarized incident wave, i.e., the t_{xx} and t_{yy} mentioned in Fig. 2, respectively. According to Eq. (7), the wavefront trajectory curves of the transmission wave at different ellipticity (i.e. ellipticity (EP) equals -0.5, -0.6, -0.7, -0.8, -0.9, and -1.0) are calculated, and

the corresponding results are illustrated in Figs. 6(b)-6(g). As we can see, when the ellipticity decreases from −0.5 to −1.0, the trajectory curves change from a flat ellipse to an ideal circle. These figures provide strong evidence of the tunable of ellipticity.

TABLE 1. Crucial performance parameters compared with the values for the historical THz polarization converters.

Reference	Efficiency	Sensitivity	Dynamic ellipticity
[21]	88% ∼ 97% (R)	——	——
[24]	< 80% (R)	——	200%
[34]	∼ 60% (T)	34 GHz/100K	30%
[35]	∼ 60% (T)	——	——
[36]	∼ 75% (T)	——	——
[37]	∼ 40% (T)	——	——
This work	88% ∼ 100% (T)	98 GHz/100K	76%

T: Transmission; R: Reflection.

Finally, performance comparison with the previously reported THz polarization converters is carried out. Table 1 displays the frequency, period, transmission efficiency, sensitivity, and dynamic ellipticity range of these converters. It can be seen that the proposed structure exhibits an improved efficiency among these reported converters. Hence, our converter represents an ultra-high transmission efficiency. Moreover, the extensive tunability of the frequency and ellipticity amplitude further exhibits the high-performance in which other converters are hardly achieved. Thus, the proposed THz polarization converters provide a promising prospect for high-efficiency THz devices.

III. CONCLUSION

In summary, we propose an ultra-high efficiency THz linear-to-circular polarization converter based on all-dielectric metasurface. Through carefully designing the structure parameters of the converter, the excellent performance is realized. In the simulation, the operating frequency of the converter ranges from 0.555 to 0.737 THz with the absolute value of AR $<$ 3 dB and efficiency $>$ 88% are achieved. The relation between geometric parameters and conversion performance provides more freedom for structural design. In addition, the InSb film is deposited on the silicon pillars to realize the tunability of the polarization converter. Numerical simulation demonstrates that the frequency sensitivity of the tunable converter can reach 98 GHz/100K, and the ellipticity can be tuned from −1.00 to −0.24 at 0.725 THz. The proposed high-efficiency and tunable polarization converters can be used as the component in THz imaging and communication devices.

ACKNOWLEDGMENT

The authors thank Lec. Ping Li from the Beijing University of Posts and Telecommunications for the manuscript revision.

REFERENCES

[1] S. Liu, A. Noor, L. L. Du, L. Zhang, Q. Xu, K. Luan, T. Q. Wang, Z. Tian, W. X. Tang, J. G. Han, W. L. Zhang, X. Y. Zhou, Q. Cheng, and T. J. Cui, "Anomalous refraction and nondiffractive bessel-beam generation of terahertz waves through transmission-type coding metasurfaces," *ACS Photon.*, vol. 3, no. 10, pp. 1968–1977, Oct. 2016.

[2] T.-T. Kim, H. Kim, M. Kenney, H. S. Park, H.-D. Kim, B. Min, and S. Zhang, "Amplitude modulation of anomalously refracted terahertz waves with gated-graphene metasurfaces," *Adv. Opt. Mater.*, vol. 6, no. 1, Nov. 2017, Art. no. 1700507.

[3] W. S. L. Lee, S. Nirantar, D. Headland, M. Bhaskaran, S. Sriram, C. Fumeaux, and W. Withayachumnankul, "Broadband terahertz circular-polarization beam splitter," *Adv. Opt. Mater.*, vol. 6, no. 3, Feb. 2018, Art. no. 1700852.

[4] L. Cong, Y. K. Srivastava, H. Zhang, X. Zhang, J. Han, and R. Singh, "All-optical active THz metasurfaces for ultrafast polarization switching and dynamic beam splitting," *Light Sci. Appl.*, vol. 7, no. 1, pp. 1–9, Jul. 2018.

[5] M. Jia, Z. Wang, H. Li, X. Wang, W. Luo, S. Sun, Y. Zhang, Q. He, and L. Zhou, "Efficient manipulations of circularly polarized terahertz waves with transmissive metasurfaces," *Light, Sci. Appl.*, vol. 8, no. 1, Jan. 2019.

[6] Q. L. Yang, X. Y. Chen, Q. Xu, C. X. Tian, Y. H. Xu, L. Q. Cong, X. Q. Zhang, Y. F. Li, C. H. Zhang, X. X. Zhang, J. G. Han, and W. L. Zhang, "Broadband terahertz rotator with an all-dielectric metasurface," *Photon. Res*, vol. 6, no. 11, pp. 1056–1061, Nov. 2018.

[7] H. F. Zhang, X. Q. Zhang, Q. Xu, Q. Wang, Y. H. Xu, M. G. Wei, Y. F. Li, J. Q. Gu, Z. Tian, C. M. Ouyang, X. X. Zhang, C. Hu, J. G. Han, and W. L. Zhang, "Polarization-independent all-silicon dielectric metasurfaces in the terahertz regime," *Photon. Res.*, vol. 6, no. 1, pp. 24–29, Jan. 2018.

[8] H. Zhang, X. Zhang, Q. Xu, C. Tian, Q. Wang, Y. Xu, Y. Li, J. Gu, Z. Tian, C. Ouyang, X. Zhang, C. Hu, J. Han, and W. Zhang, "High-efficiency dielectric metasurfaces for polarization-dependent terahertz wavefront manipulation," *Adv. Opt. Mater.*, vol. 6, no. 1, Jan. 2018, Art. no. 1700773.

[9] Y. Xu, Q. Li, X. Zhang, M. Wei, Q. Xu, Q. Wang, H. Zhang, W. Zhang, C. Hu, Z. Zhang, C. Zhang, X. Zhang, J. Han, and W. Zhang, "Spin-decoupled multifunctional metasurface for asymmetric polarization generation," *ACS Photon.*, vol. 6, no. 11, pp. 2933–2941, Oct. 2019.

[10] T.-T. Kim, S. S. Oh, H.-S. Park, R. Zhao, S.-H. Kim, W. Choi, B. Min, and O. Hess, "Optical activity enhanced by strong inter-molecular coupling in planar chiral metamaterials," *Sci. Rep.*, vol. 4, no. 1, p. 5864, Sep. 2014.

[11] T. S. Rappaport, Y. Xing, O. Kanhere, S. Ju, A. Madanayake, S. Mandal, A. Alkhateeb, and G. C. Trichopoulos, "Wireless communications and applications above 100 GHz: Opportunities and challenges for 6G and beyond," *IEEE Access*, vol. 7, pp. 78729–78757, Jun. 2019.

[12] M. Kato, S. R. Tripathi, K. Murate, K. Imayama, and K. Kawase, "Non-destructive drug inspection in covering materials using a terahertz spectral imaging system with injection-seeded terahertz parametric generation and detection," *Opt. Express*, vol. 24, no. 6, pp. 6425–6432, Mar. 2016.

[13] H.-Z. Yao and S. Zhong, "Frequency-dependent circular-polarization of terahertz chiral spoof surface plasmon polariton on helically grooved metallic wire," *Opt. Commun.*, vol. 354, pp. 401–406, Nov. 2015.

[14] Y. Wu, M. Elyasi, X. Qiu, M. Chen, Y. Liu, L. Ke, and H. Yang, "High-performance THz emitters based on ferromagnetic/nonmagnetic heterostructures," *Adv. Mater.*, vol. 29, no. 4, Jan. 2017, Art. no. 1603031.

[15] W. Liu, S. Chen, Z. Li, H. Cheng, P. Yu, J. Li, and J. Tian, "Realization of broadband cross-polarization conversion in transmission mode in the terahertz region using a single-layer metasurface," *Opt. Lett.*, vol. 40, no. 13, pp. 3185–3188, 2015.

[16] V. S. Yadav, S. K. Ghosh, S. Bhattacharyya, and S. Das, "Graphene-based metasurface for a tunable broadband terahertz cross-polarization converter over a wide angle of incidence," *Appl. Opt.*, vol. 57, no. 29, pp. 8720–8726, Oct. 2018.

[17] X. Chen, Z. Tian, Y. Lu, Y. Xu, X. Zhang, C. Ouyang, J. Gu, J. Han, and W. Zhang, "Electrically tunable perfect terahertz absorber based on a graphene salisbury screen hybrid metasurface," *Adv. Opt. Mater.*, vol. 8, no. 3, Feb. 2020, Art. no. 1900660.

[18] H. Cai, S. Chen, C. Zou, Q. Huang, Y. Liu, X. Hu, Z. Fu, Y. Zhao, H. He, and Y. Lu, "Multifunctional hybrid metasurfaces for dynamic tuning of terahertz waves," *Adv. Opt. Mater.*, vol. 6, no. 14, Jul. 2018, Art. no. 1800257.

[19] L. Y. Wang, F. Lan, Y. X. Zhang, S. X. Liang, W. X. Liu, Z. Q. Yang, L. Meng, Z. J. Shi, J. Yin, T. T. Song, H. X. Zeng, and P. Mazumder, "A fractional phase-coding strategy for terahertz beam patterning on digital metasurfaces," *Opt. Express*, vol. 28, no. 5, pp. 6395–6407, Mar. 2020.

[20] K. Bi, D. Yang, J. Chen, Q. Wang, H. Wu, C. Lan, and Y. Yang, "Experimental demonstration of ultra-large-scale terahertz all-dielectric metamaterials," *Photon. Res.*, vol. 7, no. 4, pp. 457–463, Apr. 2019.

[21] L. Zeng, T. Huang, G.-B. Liu, and H.-F. Zhang, "A tunable ultra-broadband linear-to-circular polarization converter containing the graphene," *Opt. Commun.*, vol. 436, pp. 7–13, Apr. 2019.

[22] Y. N. Jiang, L. Wang, J. Wang, C. N. Akwuruoha, and W. P. Cao, "Ultra-wideband high-efficiency reflective linear-to-circular polarization converter based on metasurface at terahertz frequencies," *Opt. Express*, vol. 25, no. 22, pp. 27616–27623, Oct. 2017.
[23] Fahad, Ruan, and Chen, "A wideband terahertz transmissive polarization manipulator based on metasurfaces," *Electronics*, vol. 8, no. 10, p. 1068, Sep. 2019.
[24] X. Yu, X. Gao, W. Qiao, L. Wen, and W. Yang, "Broadband tunable polarization converter realized by graphene-based metamaterial," *IEEE Photon. Technol. Lett.*, vol. 28, no. 21, pp. 2399–2402, Nov. 1, 2016.
[25] B. Vasić, D. C. Zografopoulos, G. Isić, R. Beccherelli, and R. Gajić, "Electrically tunable terahertz polarization converter based on overcoupled metal-isolator-metal metamaterials infiltrated with liquid crystals," *Nanotechnology*, vol. 28, no. 12, Feb. 2017, Art. no. 124002.
[26] C. Lan, H. Ma, M. Wang, Z. Gao, K. Liu, K. Bi, J. Zhou, and X. Xin, "Highly efficient active all-dielectric metasurfaces based on hybrid structures integrated with phase-change materials: From terahertz to optical ranges," *ACS Appl. Mater. Interfaces*, vol. 11, no. 15, pp. 14229–14238, Mar. 2019.
[27] Z. X. Shen, S. G. Zhou, S. J. Ge, W. Duan, L. L. Ma, Y. Q. Lu, and W. Hu, "Liquid crystal tunable terahertz lens with spin-selected focusing property," *Opt. Express*, vol. 27, no. 6, pp. 8800–8807, Mar. 2019.
[28] H. Jung, H. Jo, W. Lee, B. Kim, H. Choi, M. S. Kang, and H. Lee, "Electrical control of electromagnetically induced transparency by terahertz metamaterial funneling," *Adv. Opt. Mater.*, vol. 7, no. 2, Jan. 2019, Art. no. 1801205.
[29] D. Yang, C. Zhang, X. Li, and C. Lan, "InSb-enhanced thermally tunable terahertz silicon metasurfaces," *IEEE Access*, vol. 7, pp. 95087–95093, Aug. 2019.
[30] F. Ding, S. Zhong, and S. I. Bozhevolnyi, "Vanadium dioxide integrated metasurfaces with switchable functionalities at terahertz frequencies," *Adv. Opt. Mater.*, vol. 6, no. 9, May 2018, Art. no. 1701204.
[31] A. Cardin, K. B. Fan, and W. Padilla, "Role of loss in all-dielectric metasurfaces," *Opt. Express*, vol. 26, no. 13, pp. 17669–17679, Jun. 2018.
[32] J. Zhu, J. Han, Z. Tian, J. Gu, Z. Chen, and W. Zhang, "Thermal broadband tunable terahertz metamaterials," *Opt. Commun.*, vol. 284, no. 12, pp. 3129–3133, Jun. 2011.
[33] X.-F. Zang, S. J. Liu, H. H. Gong, Y. J. Wang, and Y. M. Zhu, "Dual-band superposition induced broadband terahertz linear-to-circular polarization converter," *J. Opt. Soc. Amer. B, Opt. Phys.*, vol. 35, no. 4, pp. 950–957, Apr. 2018.
[34] D. Wang, L. Zhang, Y. Gu, M. Q. Mehmood, Y. Gong, A. Srivastava, L. Jian, T. Venkatesan, C.-W. Qiu, and M. Hong, "Switchable ultrathin quarter-wave plate in terahertz using active phase-change metasurface," *Sci. Rep.*, vol. 5, no. 1, p. 15020, Oct. 2015.
[35] L. Zhu, L. Dong, J. Guo, F.-Y. Meng, X. J. He, C. H. Zhao, and Q. Wu, "Polarization conversion based on mie-type electromagnetically induced transparency (EIT) effect in all-dielectric metasurface," *Plasmonics*, vol. 13, no. 6, pp. 1971–1976, Feb. 2018.
[36] J. Zi, Q. Xu, Q. Wang, C. Tian, Y. Li, X. Zhang, J. Han, and W. Zhang, "Terahertz polarization converter based on all-dielectric high birefringence metamaterial with elliptical air holes," *Opt. Commun.*, vol. 416, pp. 130–136, Jun. 2018.
[37] J. Zi, Y. Li, X. Feng, Q. Xu, H. Liu, X.-X. Zhang, J. Han, and W. Zhang, "Dual-functional terahertz waveplate based on all-dielectric metamaterial," *Phys. Rev. A, Gen. Phys. Appl.*, vol. 13, no. 3, Mar. 2020, Art. no. 034042.

YANZHAO HOU (Member, IEEE) received the Ph.D. degree from BUPT, Beijing, China, in 2014. He is currently with the National Engineering Laboratory for Mobile Internet, BUPT. His current research interests include next generation wireless networks, software-defined radio, vehicular networks, and trial systems. He received the Best Demo Award in the IEEE APCC2018.

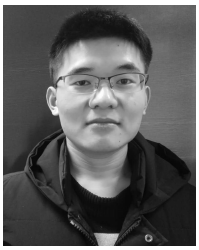

CHAO ZHANG was born in Jiangsu, China, in 1995. He received the B.S. degree in communication engineering from Nantong University, Jiangsu, China, in 2018. He is currently pursuing the M.S. degree in information and communication engineering with the Beijing University of Posts and Telecommunications. His current research interest includes THz devices.

CHENGRUI WANG was born in Henan, China, in 1997. He received the B.E. degree in communication engineering from the Beijing University of Chemical Technology, Beijing, China, in 2019. He is currently pursuing the M.E. degree in electronic and communication engineering with the Beijing University of Posts and Telecommunications.